ANSTO/External Report ER-790

Australian Government

ANSTO

Summary of Light Absorbing Carbon and Visibility Measurements and Terms.

by

David D. Cohen

Australian Nuclear Science and Technology Organisation

October 2020

ISBN – 1 921268 32 8

ISSN 1030-7745

Blank page

Abstract

This document discusses and defines the key parameters and terms that are directly related to determining the light extinction coefficient b_{ext}, light absorbing carbon (*LAC*), black carbon (*BC*) and visible range (*VR*). It provides the relationships and equations needed to determine and quantitatively measure and estimate these parameters, It discusses most of the key assumptions and corrections that researchers have applied to these parameters and it provides graphs and tables containing typical values needed in the accurate determination of these parameters.

The focus is on transmission measurements through filters used to collect fine particulate mass (PM2.5) containing carbon. There are at least two significant forms of carbon on such filters, elemental carbon (*EC*) and organic carbon (*OC*). Here we only addressed aspects associated with the measurement of elemental carbon or soot.

The document references provide a comprehensive overview of the understanding and measurement of b_{ext}, *LAC*, *BC* and *VR* and summarise the current thinking on these topics.

Contents

When citing this document please cite it as:-

David D. Cohen, Summary of Light Absorbing Carbon and Visibility Measurements and Terms. ANSTO External Report ER-790, ISBN – 1 921268 32 8, October 2020.

Blank page

1. Introduction

At ANSTO we have been measuring light absorbing carbon (*LAC*) and black carbon (*BC*) on filters for over 30 years. It is time to review and to summarise some of the key terms, equations and symbols applied to the measurement of these parameters. The filters typically have deposits of fine particulate matter (PM2.5) obtained by pulling 20 m^3 to 30 m^3 of air through them during a 24 hour period. The filters used by ANSTO were usually 25mm diameter stretched Teflon or 47mm polycarbonate Nuclepore filters but the principles discussed here are directly applicable to other types of filters.

The focus of this document is on photon transmission measurements through these filters, at various wavelengths, to obtain estimates of light extinction coefficient (b_{ext}), *LAC*, *BC* and visible range (*VR*).

In the reference section of this document we have alphabetically listed a range of key references [1-27] which are directly related to the arguments and discussions presented in the document. If read they will provide a comprehensive review and a deeper understanding of this field of research related to light transmission measurements for determining the carbon content on filters. This document will assume that these references have been read in detail and we will not be reproducing many of the concepts and ideas developed over the decades. It will be assumed that the reader does have at least a basic knowledge and understanding of this field.

A full list of terms and symbols used here are defined in Appendix 1.

2. Extinction Coefficients

Back in 1990 at ANSTO we started with the following equations to determine extinction coefficients b_{ext} and the black carbon content of our filters [1,8-10].

$$b_{ext} = (b_{abs} + b_{scat})_{part} + (b_{abs} + b_{scat})_{gas} \qquad 2.1$$

Note that b_{abs} for particles is often just written as b_{ap}, similarly b_{scat} for gases is sometimes written as b_{sg} which is often referred to as Rayleigh gas scattering. Typically, for air at sea level b_{sg}~10Mm^{-1} and b_{sp} is greater than b_{abs} and b_{ag} is mainly due to atmospheric NO_2 gas. The most significant absorption is in the 400nm to 500nm range and at typical ambient concentrations, absorption by NO_2 does not contribute significantly to the atmospheric extinction. The value of b_{ap} is quite variable and hard to estimate *a priori*.

The particle scattering albedo is defined as [8,24],

$$\omega_0 = \left[\frac{b_{sp}}{(b_{ap}+b_{sp})}\right] = 1 - \left[\frac{b_{ap}}{b_{ext}}\right] \qquad 2.2$$

Fig. 2.1 shows the single scattering albedo against particle diameter [8-10] for a) solid particle with density 2.25g/cm^3 and a complex refractive index [6] *m=2.0-1.0i*, b) a 50%

solid particle with density 1.5 g/cm^3 and refractive index *m=1.5-0.01i*, and c) a 50% solid particle with density 1.25g/cm^3 and refractive index *m=1.5-0.5i*.

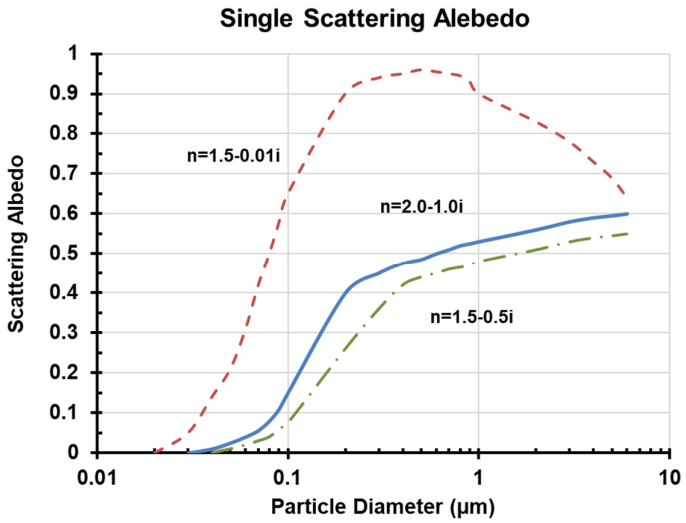

Fig. 2.1. *Single particle scattering albedo plot against particle diameter for different particle refractive indices.*

Typical particle refractive indices[3,8] are given in Table 2.1 where *m=n-ik* and λ=500nm. Note that *n* and *k* are wavelength dependent.

Table 2.1. Refractive indices for typical particles at λ=500nm [1-6,20]

Substance	*n*	*k*	ρ(g/cm^3)
Water	1.33	0	1.00
Haematite Fe_2O_3	2.6	1.0	5.3
Graphite (solid)	2.0	1.0	2.25
Elemental carbon	1.80	0.54	1.50
Organic matter	1.55	0.001	1.4
NaCl (solid)	1.54	0	2.16
H_2SO_4 (aqueous)	1.53	0	1.83
$(NH_4)_2SO_4$ (solid)	1.52	0	1.77
NH_4NO_3 solid	1.54	0	1.725
SiO_2	1.55	0	2.65
Sydney PM2.5 summer [4]	1.46	0.05	1.6-1.8
Sydney PM2.5 winter [4]	1.46	0.23	1.6-1.8

The real part *n* is responsible for scattering and the imaginary part *k* for absorption.

The most important light absorbing particles are those of elemental carbon or black carbon (*BC*), light absorbing carbon (*LAC*) and graphitic soot.

The Beer Lambert law for transmission through a thickness *x* of a material of density ρ is [8],

$$I = I_0 e^{-\left(\frac{\mu}{\rho}\right)\rho x} \qquad 2.3$$

The mass absorption coefficients (in m^2/g) are a function of atomic number *Z* of the absorbing material and the wavelength (λ) of the radiation,

$$\left(\frac{\mu}{\rho}\right) = aZ^b\lambda^c \qquad 2.4$$

where *a, b and c* are constants.

The Beer Lambert law can also be rewritten as [24],

$$I = I_0 e^{-b_{ext}x} = I_0 e^{-\tau} \qquad 2.5$$

where I_0 is the initial intensity and I the final intensity after traveling a distance *x* or ρx in a material and τ is called the aerosol optical depth.

Note this is a single scattering approximation.

b_{ext} is measured in units of Mm^{-1} or sometimes just $(10^4 m)^{-1}$ and is given by [24].

$$b_{ext}(Mm^{-1}) = 100\left[\frac{A(cm^2)}{V(m^3)}\right] ln\left[\frac{I_0}{I}\right] \qquad 2.6$$

where *A* is the collection area on the filter, *V* is the volume passed through the filter. Note we include the units used to avoid confusion and to be consistent through all equations and symbols used here.

For black carbon particles on a filter we assume $b_{ext} \sim b_{abs}$ and end up with the familiar approximate equation [5,7],

$$b_{abs}(Mm^{-1}) = \left[\frac{100A(cm^2)}{V(m^3)}\right] ln\left[\frac{I_0}{I}\right] \qquad 2.7$$

which we have used to estimate b_{abs} by measuring the transmission/ absorption of particles collected on a filter paper.

Often the symbol *ATN* is used [1,2,7,5,24] to replace the log of the intensities term, that is,

$$ATN = 100ln\left[\frac{I_0}{I}\right] = -100ln\left[\frac{I}{I_0}\right] \qquad 2.8$$

At ANSTO we have avoided the use of these extra symbols and definitions as they generally add little and can be confusing at times if defined differently by different users.

Over the decades many researchers have made major corrections to the b_{abs} measurement. A correction *C* for the multiple scattering that occurs for a filter when trying to determine *I* from I_o in a transmission experiment. This is necessary because light scattered out of the filter can actually be misinterpreted as losses due to absorption in the filter [2,23]. It is for this reason we use the opaque glass in our MABI units to scatter the scattered light back through the filter to the detector. It is also the reason why the filter deposit should face the detector and not the light source in our MABI unit. A layer loading

or shadowing correction *R* is also often applied when the filters are heavily loaded. *R* is a function of the filter loading or thickness *(ρx)*. The need for this correction has never been entirely clear [9] as after all we are using the Beer Lambert law to measure absorption essentially as a function of thickness. Horvath [8-10] agrees that this correction should not be necessary. Nevertheless, it seems to be accepted practice for converting some integrating plate and some aethalometer readings to b_{abs} readings as these instruments show a need to correct deposit thicknesses after each successive reading [2,23,24].

We define the corrected b_{abs} as [24],

$$b_{abs}^{corr}(Mm^{-1}) = C\left[\frac{b_{abs}(Mm^{-1})}{R[\rho x(\mu g\, cm^{-2})]}\right] \qquad 2.9$$

In the early days (1990s) we used this $b_{abs}^{corr}(Mm^{-1})$ equation to estimate b_{abs} from our Teflon filters. Our values of *C* and *R* were taken from the UCD IMPROVE stretched Teflon values, namely,

$$C=0.97 \text{ and,} \qquad 2.10$$

C is filter type and site specific [1].

$$R(\rho x) = 0.36exp\left[\frac{-\rho x}{22}\right] + 0.64exp\left[\frac{-\rho x}{415}\right] \qquad 2.11$$

where *(ρx)* in μg/cm^2 is the deposit thickness on the filters, given by,

$$\rho x(\mu g cm^{-2}) = CMass\ (\mu g m^{-3}) * \left[\frac{Vol(m^3)}{A(cm^2)}\right] \qquad 2.12$$

Researchers using aethalometers [2,3,5,7,14,23,24] generally express their laying correction *R* in terms of *ATN* and a dimensionless compensation parameter called *k*. That is,

$$R[\rho x(\mu g cm^{-2})] = (1 - k * ATN) = \{1 - 100k * ln\left[\frac{I_0}{I}\right]\} \qquad 2.14$$

Rearranging this equation we see that *k* would be related to the IMPROVE *R* by,

$$k = \left[\frac{1-R(\rho x)}{ATN}\right] = \left[\frac{1-R(\rho x)}{100ln\left[\frac{I_0}{I}\right]}\right] \qquad 2.15$$

In the Fig. 2.2 below we plot *R* as a function of *CMass*. For *CMass*=10 μg/m^3 the correction *R*=0.46 and for *CMass*=50 μg/m^3 it is *R*=0.12. Hence the *R* correction would tend to increase the b_{abs} measurements by a factor of between 2 to 8 for most situations in the ASP network for the Sydney region depending on the filter loading.

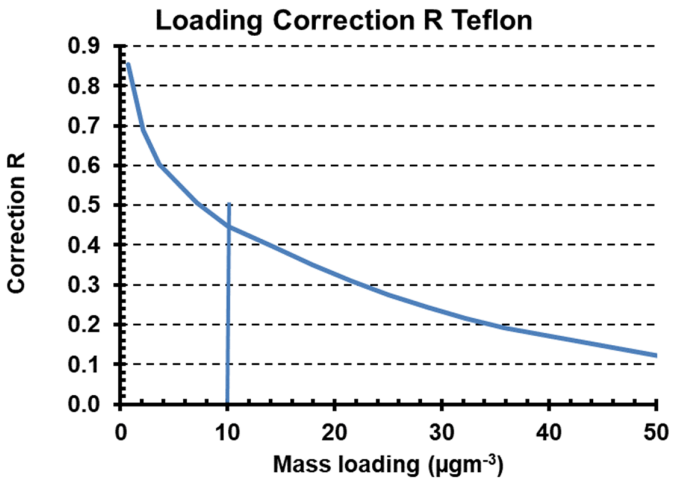

Fig.2.2 *The R layer correction with CMass for Teflon filters.*

The average *R* values for our ASP network range from *R*=0.33 in Hanoi, Vietnam to *R*=0.57 at Broome, WA. The corresponding average *k* values are much smaller and for our ASP network range from *k*=0.0040 at Hanoi to *k*=0.0087 at Stockton, NSW.

Note that b_{abs} is related to the mass absorption coefficient ϵ(m²/g) and the mass absorption cross section σ_{abs}(cm²) by,

$$b_{abs}(Mm^{-1}) = \rho(g/cm^3) * \epsilon(m^2/g) = \sigma_{abs}(cm^2)/V(m^3) \qquad 2.16$$

where ρ is the particle density and *V* is the volume of collected particles. The current accepted fine particle density is around 1.8 g/cm³ rather than the old traditionally excepted value closer to 1 g/cm³.

Often is useful to calculate the number of particles/ unit volume *N* for a given gas or material,

$$N(particles/cm^3) = \left[\frac{N_0 \rho(g/cm^3)}{W(g)}\right] \qquad 2.17$$

Where N_0 =6.022141x10²³ is Avogadro's number and W is the atomic weight of the species with density ρ.

3. Light Absorbing Carbon (LAC)

Now we have a method for measuring b_{abs} we can convert this to a light absorbing carbon (*LAC*) concentration measurement (in ng/m³) using an uncorrected mass absorption coefficient ϵ and the transmission measurement techniques.

$$LAC(ng/m^3) = 1000\left[\frac{b_{abs}^{corr}(Mm^{-1})}{\epsilon(m^2/g)}\right] \qquad 3.1$$

or in terms of the transmission intensities before and after filter exposure,

$$LAC(ngm^{-3}) = \frac{10^5 C*[A(cm^2)]}{[\epsilon\,(m^2g^{-1})]*R*[V(m^3)]} ln\left[\frac{I_0}{I}\right] \quad 3.2$$

It is important to note at this point that we could define a corrected mass absorption coefficient,

$$\varepsilon^{corr}(m^2g^{-1}) = \epsilon(m^2g^{-1}) * \left[\frac{R}{C}\right] \quad 3.3$$

This is in effect what we have done since 1998 when we set *C*=*R*=1.0, stopped using the mass attenuation coefficient ϵ=10 m^2/g accepted by the UCD IMPROVE network and measured our own mass attenuation coefficients using our HeNe laser system (λ=633nm) and performing soot from candles and acetylene torch experiments. From 1998 onwards we measured and have used ε^{corr}=7m^2/g for all Teflon filters measured using our HeNe laser system [20].

Note we will use two different but similar symbols to represent the mass absorption coefficient. The uncorrected one is ϵ and the corrected one is ε.

This correction in effect means that our mass attenuation coefficients will be smaller by a factor [*R/C*] than for instance those used in standard aethalometer systems as we do not directly make these corrections but have absorbed them into the ε^{corr} value itself. For example, Magee AE33 aethalometers [Magee User Manual March 2016, https://www.manualslib.com/manual/1376483/Magee-Scientific-Aethalometer-Ae33.html] quote their ϵ at a wavelength of 660nm as 10.35m^2/g which if equated to our 7 m^2/g at 633nm implies a [R/C]= 0.67 consistent with the mass loading (*CMass*~2.5μg/m^3) and scattering corrections for Teflon filters discussed above. Nowadays we just set C=R=1.0 in the equations above and talk about the mass absorption coefficient as being ε without the *corr* superscript.

For completeness the equations are included that would be used for reflection measurements of LAC such as would be done using a Smoke Stain Reflectometer. This instrument uses a broad band white light source with an average wavelength λ=550nm.

$$LAC(\mu gcm^{-2}) = \frac{100}{[2\epsilon\,(m^2g^{-1})]} ln\left[\frac{R_0}{R}\right] \quad 3.4$$

where R_0 and R are the initial and final reflected intensities similar to I_0 and I. The factor of 2 in the denominator reflects the increased white light pathlength both in and out of the filter material.

Note that usually R_0 is set to 100% then *R%* is defined by [5],

$$\%R = \left[\frac{100R}{R_0}\right] \; with\; R_0\text{=}100\% \quad 3.5$$

Maenhaut [13] defines an empirical LAC for Nuclepore fine filters as,

$$LAC(\mu g cm^{-2}) = \frac{100}{[2\epsilon\,(m^2 g^{-1})]}\{4.605 - ln[\%R]\} \quad 3.6$$

In 2017 the ASP program moved away from HeNe laser transmission (at 633nm) measurements for *LAC* to our newly developed MABI instrument using seven different wavelengths from 405nm to 1050nm. Comparison measurements between HeNe laser and MABI provided a ε(MABI) = 6.44m^2/g at 639nm to provide identical *LAC* measurements with the HeNe laser ε(HeNe)=7m^2/g at 633nm.

It should be noted that *LAC* by its nature is an estimate only of the black carbon content on the filter. It depends on other chemical species on the filter that change its 'blackness' and hence the transmission properties of the loaded filters.

Earlier work by UCD in the USA National Parks IMPROVE program [12] made a correction to *LAC* for the soil content on the filter as this reduced its blackness. We have used this same correction on *LAC* since 1990 to define our black carbon (BC) estimates namely,

$$BC(\mu g/m^3) = LAC(\mu g/m^3) - 0.11*Soil(\mu g/m^3) \quad 3.7$$

where,

$$Soil = 2.20*[Al] + 2.49*[Si] + 1.63*[Ca] + 1.94*[Ti] + 2.42*[Fe] \quad 3.8$$

and the oxides of Al, Si, Ca, Ti and Fe have been assumed. The [Fe] concentration is assumed to be 50% FeO and 50% Fe_2O_3. These five metal oxides on average account for only 86 % of the average soil composition so each of the coefficients has been multiplied by 1.16 to account for this.

It should be noted that in the ASP program when we use *BC* for black carbon we are talking about a soil corrected *LAC*.

4. Measurement of Mass Attenuation Coefficients

The variability of the mass attenuation coefficient (often referred to in publications as *MAC*) with wavelength is [1,8],

$$\varepsilon(\lambda) = a\lambda^{-\alpha} \quad 4.1$$

where *a* and α are constants. In generally accepted Mie theory the exponent α, sometimes called the Angstrom exponent [24,26], is α=1 for *BC* from high temperature fossil fuel combustion and α=2 for biomass or wood burning. This is strongly dependent on a range of parameters including *BC* particle refractive index [6], the *BC* core diameter and particle density. Generally, for our MABI systems 0.4<α<1. This value of α lower than unity implies that the *BC* particles we generally measure have core diameters in the range 150nm to 200nm rather that the much smaller range below 150nm where α would be closer to or above unity.

Wu et al [26] point out that this exponent varies with particle core diameter and whether or not the particles are coated. Fig.4.1 shows an example of this variation for non-coated black carbon particles with a range of core diameters.

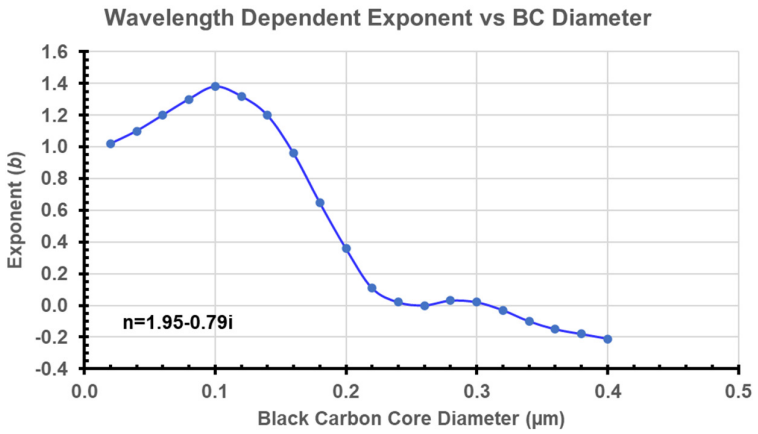

Fig.4.1. Variation of the absorption exponent b of non coated black carbon particles with a refractive index of m=1.95-0.79i. Adapted from Wu et al 2015.

To estimate a $\varepsilon(\lambda)$ as a function of wavelength we measure *LAC* at each of the seven different MABI wavelengths. At two wavelengths λ_1 and λ_2 we have the ratio of *LAC*s is given by,

$$\frac{LAC(\lambda_2)}{LAC(\lambda_1)} = \left[\frac{\varepsilon(\lambda_1)}{\varepsilon(\lambda_2)}\right] \frac{ln\left[\frac{I_0(\lambda_2)}{I(\lambda_2)}\right]}{ln\left[\frac{I_0(\lambda_1)}{I(\lambda_1)}\right]} \qquad 4.2$$

Rearranging and solving for $\varepsilon(\lambda_2)$ as a function of $\varepsilon(\lambda_1)$ a known mass attenuation coefficient we get,

$$\varepsilon(\lambda_2) = \varepsilon(\lambda_1) \left[\frac{LAC(\lambda_1)}{LAC(\lambda_2)}\right] \frac{ln\left[\frac{I_0(\lambda_2)}{I(\lambda_2)}\right]}{ln\left[\frac{I_0(\lambda_1)}{I(\lambda_1)}\right]} \qquad 4.3$$

Assuming that $LAC(\lambda_1) = LAC(\lambda_2)$ then the gradient of a linear plot of $ln\left[\frac{I_0(\lambda_2)}{I(\lambda_2)}\right]$ against $ln\left[\frac{I_0(\lambda_1)}{I(\lambda_1)}\right]$ at the two different wavelengths will provide the required estimate of $\epsilon(\lambda_2)$.

For our MABI system we use the middle wavelength λ_1=639nm and assume $\epsilon(\lambda_1)$. = 6.44m^2/g to obtain our $\varepsilon(\lambda_2)$ for each of the seven MABI wavelengths.

Fig. 4.2 shows a typical MABI linear plot of $ln\left[\frac{I_0(\lambda_2)}{I(\lambda_2)}\right]$ against $ln\left[\frac{I_0(\lambda_1)}{I(\lambda_1)}\right]$ for λ_1=639nm and λ_2=940nm.

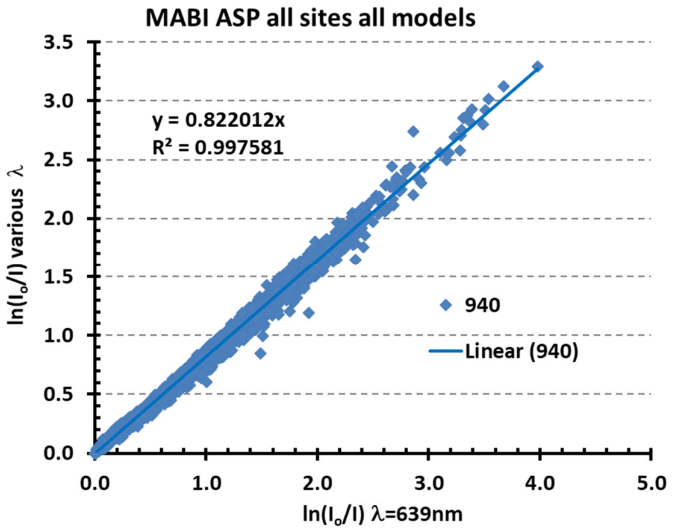

Fig. 4.2. A plot for two different wavelengths λ=940nm and 639nm of the log of the attenuation intensities for thousands of stretched Teflon filter.

The gradient for the fit at 639nm to 940nm for over 4,300 fine Teflon filters was 0.822 so if $\varepsilon(\lambda_1=639\text{nm})=6.44$ m^2/g then $\varepsilon(\lambda_2=940\text{nm})=0.822*6.44=5.29$ m^2/g. This process is repeated for each of the seven MABI wavelengths and a plot of $\varepsilon(\lambda)$ against wavelength produced. Fitting this curve to a power law gives the variation of the mass attenuation coefficient with wavelength as shown in Fig. 4.3 for different filter types.

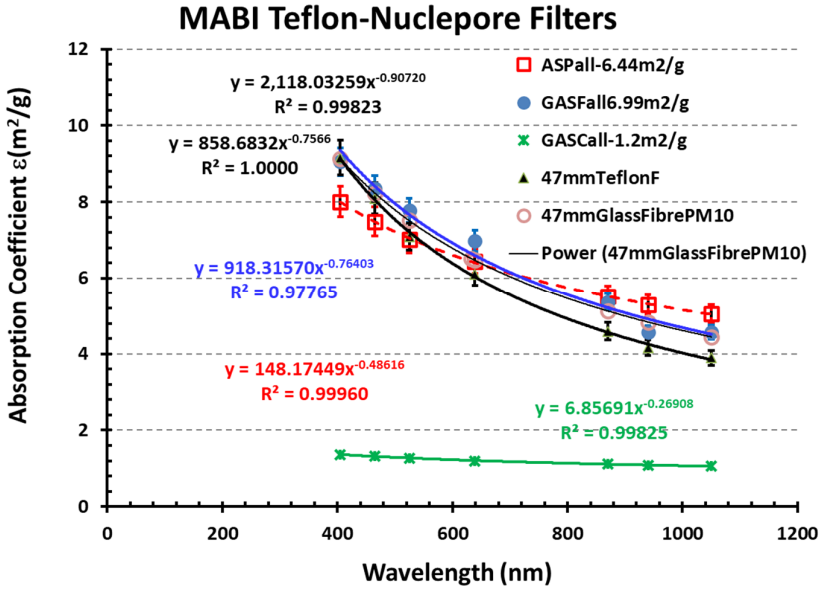

***Fig. 4.3.** Measured corrected mass attenuation coefficients for a range of wavelengths and for different filter types.*

The ASP all curve is for 25mm stretched Teflon filters, the GASF all for 47mm fine Nuclepore filters, GASC all for 47mm coarse Nuclepore filters and the 47mm Glass for 47mm glass fibre filters used in PM10 mode.

The data in Fig. 4.3 has been summarised in Table 4.1 and the coefficients *a* and α provided for each filter type.

Table 4.1. *Measured corrected mass attenuation coefficients for a range of wavelengths and for different filter types.*

Fitted Coefficients					
a	148.17449	918.3157	6.8569	2118.0326	858.6832
α	0.48616	0.76403	0.26908	0.90720	0.75664
Mass Absorption Coefficient ε (m^2/g)					
λ(nm)	**25mm Stretched Teflon (Fine PM2.5)**	**Polycarbonate 47mm Nuclepore Filter (Fine PM2.5)**	**Polycarbonate 47mm Nuclepore Filter (Coarse PM2.5-10)**	**47mm Teflon Filter (Fine PM2.5)**	**Whatman 47mm Glass Fibre GF/A 1.6µm PM10**
405	8.001	9.350	1.363	9.130	9.140
465	7.481	8.414	1.313	8.054	8.232
525	7.052	7.668	1.271	7.214	7.510
633	6.439	6.647	1.209	6.088	6.519
639	6.410	6.599	1.206	6.036	6.473
870	5.517	5.213	1.110	4.562	5.125
940	5.313	4.914	1.087	4.253	4.833
1050	5.035	4.516	1.055	3.847	4.445

It is pointed out again that the mass attenuation coefficients plotted in Fig. 4.3 and presented in Table 4.1 are the corrected ε^{corr} values. Since the scattering corrections *C* and the loading corrections *R* are implicit in these data, and are different for each filter type in a transmission type experiment, we would expect the power curves of Fig. 4.3 to be similar but show different wavelength dependence.

All the ASP program b_{abs}, *LAC* and *BC* data reported using our MABI transmission system use data at a wavelength λ=639nm obtained.

5. Stretched Teflon Thickness Measurements

ASP has used 25mm diameter stretched Teflon filters for decades. These filters typically weigh around 45mg each and have a normal thickness of 250 µg/cm^2. We have run these blank unexposed filters through our MABI system to obtain typical ranges of I_0 readings We have cut out the central 21mm diameter stretched Teflon from its sold ring support and weighed it. On average the central stretched portion of each filter is only 2 to 3% of the total filter weight. The bulk of the filter weight being in its support ring.

This technique enables us to obtain an empirical relationship between the Teflon thickness *Thk*(µg/cm^2) and the associated $\boldsymbol{I_0}$ reading for that filter namely,

$$Thk(\mu g/cm^2) = -ln\left[\frac{I_0(639nm)}{0.820226}\right]/1.50783x10^{-3} \qquad 5.1$$

This equation is valid for Teflon filter thicknesses 150µg/cm^2<*Thk*<450µg/cm^2 and has been applied to all Teflon filter thickness determinations from January 2017 onwards. It is called the I_0 method for filter thickness determination.

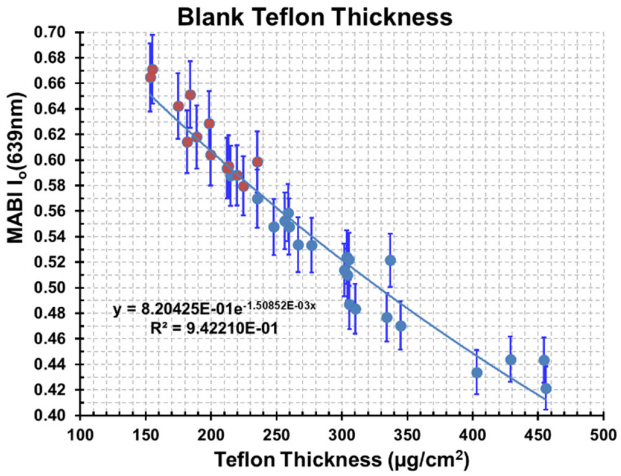

Fig. 5.1 *Plot of the MABI I_o reading at 639nm against the stretched Teflon gravimetric mass thickness (µg/cm^2).*

If each filter Teflon is $(CF_2)_n$ then its I_0 transmission intensity can also be used to determine the carbon and fluorine content of each individual filter which can then be used as a calibration standard for RBS carbon measurements and PIGE fluorine measurements in our IBA analysis of these filters. Each Teflon filter is 24% carbon and 76% fluorine. IBA analysis shows that each Teflon filter is extremely pure with very low concentrations of any trace elements. So the assumption that Teflon is just carbon and fluorine is an excellent one.

6. Mie Theory for Light Absorbing Black Carbon

Mie theory for fine particles defines the mass absorption coefficient $\varepsilon(\lambda)$ as a function of wavelength as [3,6,8],

$$\varepsilon(\lambda) = \frac{3\pi Q(x)}{2(x\rho\lambda)} \qquad 6.1$$

where,

$$x = \left[\frac{\pi D}{\lambda}\right] \qquad 6.2$$

and D is the particle aerodynamic diameter, λ the wavelength of the absorbing light, ρ the particle density. $Q(x)$ is the normalised efficiency factor and generally,

$$Q_{ext}(x) = Q_{scat}(x) + Q_{abs}(x) \qquad 6.3$$

If $x<<1$ then we are in the Rayleigh scattering regime and $Q_{scat} \propto \lambda^{-4}$ and $Q_{abs} \propto \lambda^{-1}$, if $x>>1$ in the large particle regime then $Q_{scat} \propto x$ and independent of wavelength λ.

More generally for *i=ext, scat or abs* the normalise efficiency factor Q_i is [8],

$$Q_i = \left[\frac{4\sigma_i}{\pi D^2}\right] \qquad 6.4$$

where σ_i is the extinction, scattering or absorption cross section, usually measured in units of cm^2.

In terms of the complex refractive index $m = n - ik$, discussed above Mie theory for spherical particles of diameter D and density ρ gives [3,6],

$$b_{abs}(Mm^{-1}) = \left[\frac{\sigma_{abs}(cm^2)}{V(cm^3)}\right] = \left(\frac{6\pi}{\lambda}\right) Imag\left[\frac{(m^2-1)}{(m^2+2)}\right] \qquad 6.5$$

where $\sigma_{abs}(cm^2)$ is the absorption cross section and,

$$\left[\frac{b_{abs}}{CMass}\right] = \left[\frac{3Q_{abs}}{2D\rho}\right] \qquad 6.6$$

and *CMass* is the mass per unit volume.

A similar expression can be obtained for b_{scat} namely [3],

$$b_{scat}(Mm^{-1}) = \left[\frac{\sigma_{scat}(cm^2)}{V(cm^3)}\right] = \left(\frac{4\pi^4 D^3}{\lambda^4}\right)|(m^2-1)/(m^2+2)|^2 \qquad 6.7$$

So if you know the refractive index (m) and density of particles you can calculate their b_{abs} and hence their *LAC* contributions using Mie theory [6]. These Mie theory estimates are generally significantly lower than the measured experiment values [3]. This is due mainly to the assumptions Mie theory uses, such as spherical hard particles with known aerodynamic diameters.

There are two distinct regions [20] for $\epsilon(\lambda)$ depending on whether D is greater than of less than λ, namely,

$$\varepsilon(\lambda) \sim \left[\frac{3}{2D\rho}\right] \quad for\ D > \lambda/\pi\ and\ Q(x) \sim 1 \qquad 6.8$$

For large particle diameters $Q(x) \sim 1$ making the mass absorption coefficient inversely proportional to the particle diameter and its density ρ. For small particle diameters $Q(x)$ is proportional to ax where a is a constant and,

$$\varepsilon(\lambda) \sim \left[\frac{3\pi a}{2\lambda\rho}\right] \quad for\ D < \lambda/\pi, and\ Q(x) \sim ax \qquad 6.9$$

For $D<(\lambda/\pi)$ the mass absorption coefficient is a constant independent of particle diameter D for given wavelength and particle density. But is inversely proportional to the wavelength of the absorbing light and the particle density ρ.

The MABI unit uses seven wavelengths λ=405nm, 465nm, 525nm, 639nm, 870nm, 940nm and 1050nm so it essentially samples different particle sizes.

Fig. 6 shows typical Mie theory calculations for the mass absorption coefficient (m^2/g) as a function of particle diameter for different particle densities ρ and particle refractive indices n for a given wavelength λ=633nm. The refractive index $m=n-ik$ is complex, where the dispersive extinction coefficient k is the complex absorption part. A solid carbon particle might have density ρ=2.25 g/cm^3 and k=1.0 giving a complex refractive index of around $m=2.0-1.0i$. For the same graphite particle which is 50% hollow k=0.5 and the complex refractive index m=1.5-0.5i and a density of ρ=1.25g/cm^3. Light absorbing carbon aerosols with a mass absorption coefficient ε=7m^2/g at λ=633nm have a complex refractive index $m=1.75-0.5i$ with a density ρ=0.85g/cm^3. Whereas smoke from a candle might have density ρ~1.6 g/cm^3 and a complex refractive index of around m~$1.8-0.7i$.

Fig. 6.1 clearly demonstrates the two regions defined by the particle diameter [20]. For large diameter particles $D>(\lambda/\pi)$=200nm the mass absorption coefficient falls off inversely with the particle diameter D whereas for particle diameters $D<(\lambda/\pi)$=200nm the mass absorption coefficient is essentially independent of the particle diameter D at between 4 and 9 m^2/g depending on the particle density and its refractive index.

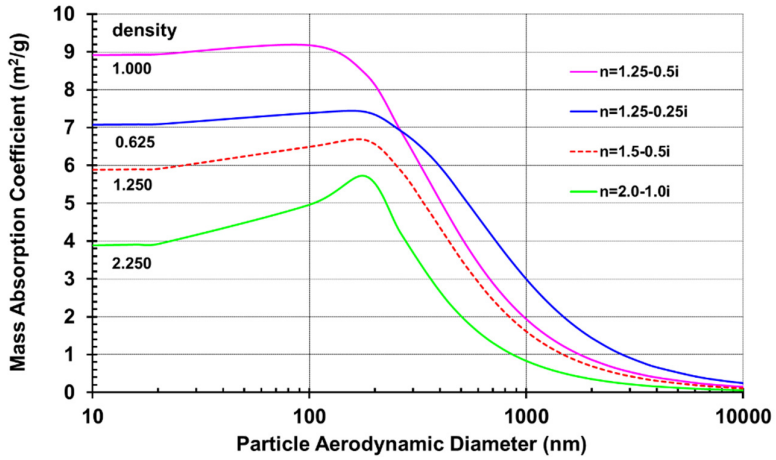

Fig. 6.1. *Mass absorption coefficient as a function of particle aerodynamic diameter for a given wavelength λ=633nm and range of particle densities and refractive indices.*

For particle densities between 0.5 and 1.5 g/cm^3, Fig.6.1 shows that the mass absorption coefficient ε(m^2/g) would be between 5 m^2/g and 8 m^2/g.

Fig. 6.2 Shows a scanning electron microscope image of carbon black particles collected on a PM2.5 stretched Teflon filter. The roughly spherical particles are black carbon and the long fibres are the stretched Teflon filter fibres. The bottom right hand shows a typical 1µm bar, clearly individual carbon spheres are well below 2.5 µm in diameter. The majority of individual spheres are indeed below 300nm in diameter.

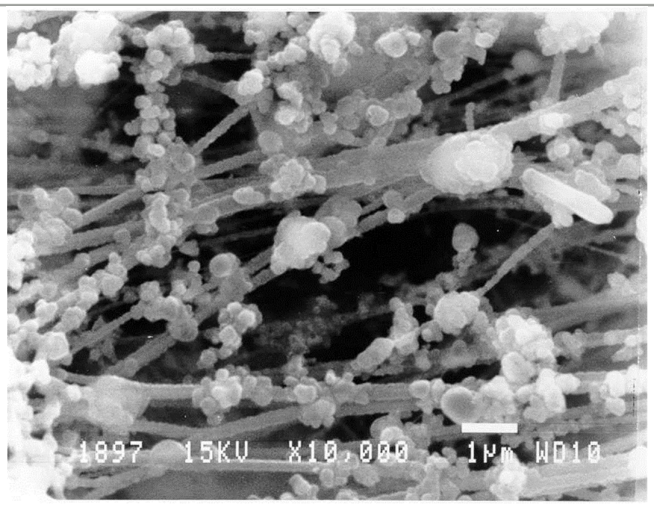

Fig.6.2. *SEM picture of black carbon on stretched Teflon filters sampling PM2.5 particles.*

7. Smoke Signatures and LAC

The MABI unit measures *LAC* at a range of wavelengths from 405nm < λ < 1050nm this means it is responsive to a range of different particle diameters. *LAC* particles formed at high temperatures, such as in fossil fuel combustion in diesel vehicles, are generally small 100nm to 300nm in diameter, solid and spherical in nature. Whereas *LAC* particles formed at lower temperatures, such as in biomass burning in wood heaters and bushfires, can be larger, non-spherical and even hollow. These two types also absorb at different wavelengths and have different densities and refractive indices. Carbon generated by high temperature combustion absorbs more in the infrared whereas low temperature carbon absorbs at shorter wavelengths. This means they have different wavelength dependent b_{abs} values.

Fig.7.1 shows this difference for b_{abs} measured at several Sydney Basin sites on over 3,000 sampling days when they were strongly influenced by biomass burning, smoke and when there was little smoke and mainly fossil fuel combustion from motor vehicles or diesel smoke present. The indicator used to determine these two regimes was,

$$Smoke(\text{ng/m}^3) = LAC(\lambda=405\text{nm}) - LAC(\lambda=1050\text{nm}) \qquad 7.1$$

Clearly, the b_{abs} due to biomass burning is larger at shorter wavelengths than the b_{abs} due to fossil fuel combustion at longer wavelengths. The power laws are also different with different exponents. For fossil fuel and diesel smoke the b_{abs} exponent was $\alpha_{ff} = 0.473$, while for biomass burning or bushfire smoke $\alpha_{bb} = 1.15$. The total b_{abs} had an exponent of $\alpha = 0.949$. Note these exponent values for smoke from fossil fuel burning and biomass burning are both below the expected Mie theory values of $\alpha_{ff}=1.0$ and $\alpha_{bb}=2.0$. Possible reasons for this have been discussed in the section above on *Light Absorbing Carbon (LAC)*.

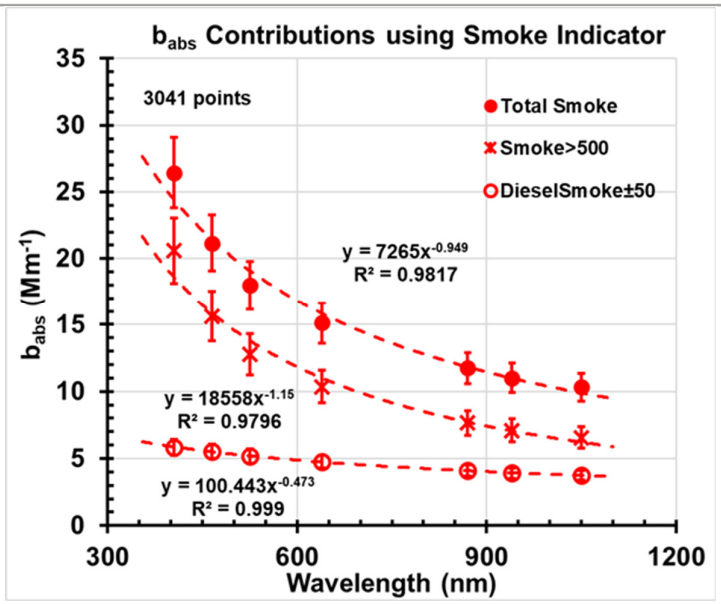

Fig.7.1. *b_{abs} (Mm^{-1}) vs wavelength for days when smoke >500 ng/m^3 and when diesel smoke<±50 ng/m^3.*

This difference in *LAC* between the short λ=405nm and the long λ =1050nm wavelength measurements can clearly be used to differentiate smoke from low temperature biomass burning over smoke from higher temperature fossil fuel burning.

Fig. 7.2 shows a plot of the normal *LAC* at the Richmond site in NSW at 639nm. It also shows the smoke indicator, *Smoke*(ng/m^3), as defined above for the same time period.

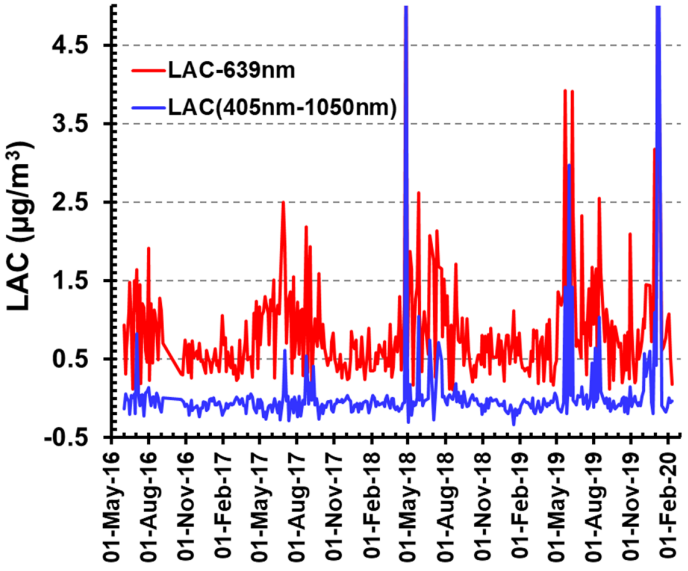

FIG. 7.2. *shows the PM2.5 LAC estimates for our Richmond sampling site from May 2016 to Feb 2020 at λ = 639nm and 405-1050nm.*

.If the *LAC* was all from high temperature fossil fuel combustion products with small diameters (*D*<300nm) then we would expect this smoke indicator data to be essentially zero The fact that we have large positive peaks on some days shows that on these days the *LAC* was from biomass burning with different particle diameters and different absorption properties. Note also that this smoke indicator can be negative, it is just its average value that we expect to be zero. That is why we defined diesel smoke to be less than or equal to ±50ng/m^3.

8. Visibility

The visual range (*VR*) in kilometres is defined as a function of light extinction b_{ext} as [17,19,25,27],

$$VR\ (km) = \left[\frac{1000ln\left[\frac{1}{0.02}\right]}{b_{ext}(Mm^{-1})}\right] = \left[\frac{3{,}912}{b_{ext}(Mm^{-1})}\right] \qquad 8.1$$

The 0.02 term represents the contrast threshold of the human eye as well as on the inherent contrast of the visible object against the horizon sky. Here we assume this threshold contrast is 2%.

The visual range has been found in a number of cases to be directly related to the fine particle mass concentrations. In 2007 Pitchford et al [17] developed a refined algorithm for light extinction coefficients b_{ext} as a function of measured chemical species. This algorithm was complicated and based on 15 variables such as sulfate, nitrate, organic matter, soil, dust and sea salt. They used fine and coarse particle data from extensive measurements from the IMPROVE program operating in National Parks across North America.

Pitchford's algorithm relates measured chemical concentrations to b_{ext},

$$\begin{aligned} b_{ext} = {} & 2.2f_S(RH)*[\text{Small Sulfate}] + 4.8f_L(RH)*[\text{Large Sulfate}] + \\ & 2.4f_S(RH)*[\text{Small Nitrate}] + 5.1f_L(RH)*[\text{Large Nitrate}] + \\ & 2.8\,[\text{Small Organic Mass}] + 6.1\,[\text{Large Organic Mass}] + \\ & 10\,\text{Elemental Carbon} + \text{Fine Soil} + 1.7f_{SS}(RH)*[\text{Sea Salt}] + \\ & 0.6\,\text{Coarse Mass} + \text{Rayleigh Scattering (Site Specific)} + \\ & 0.33\,[NO_2\ (ppb)] \end{aligned} \qquad 8.2$$

where $f_{L,S,SS}(RH)$ are water growth factor that are a function of relative humidity for small and large particles for sulfate, nitrate and sea salt. In order to utilize this algorithm, substantial additional data is required including NO_2 and Cl concentrations and a more complex relative humidity.

This algorithm is fairly complicated and requires many different chemical species concentrations as well as relative humidity measurements. Yi et al [25] have simplified this model and related visibility and b_{ext} to just 3 parameters, PM2.5 mass (*CMass* in µg/m^3), relative humidity (*RH*) and the NO_2 concentration (µg/m^3). Their Model I defines visibility through the equation,

$$\left[\frac{-ln\,(0.02)}{VR(km)}\right] = a * [CMass] * (1 - 0.01 * RH)^b + c*[NO_2] + d \qquad 8.3$$

where *a*=0.00143, *b*=-1.10731, *c*=-0.00073 and *d*=0.21376. Note the *b* and *c* coefficients are negative. The parameters in [ ] brackets are concentrations in air in (µg/m^3). Normally the NO_2 concentrations are small, measured in parts per hundred million (pphm) and have little effect (usually less than 2%-3%) on the final calculated visibility range *VR*.

As [NO_2] concentrations are usually measured in pphm the conversion in air at 20^{o}C assuming the density of air is 1.2041 kg/m^3 is,

$$[NO_2] \text{ in } \mu g/m^3 = 12.041*[NO_2] \text{ in pphm} \qquad 8.4$$

As *CMass* and [NO_2] approach zero and in low *RH* conditions $VR \rightarrow -ln(0.02)/d = 18$ km. This visible range is low for Sydney so we have adjusted to *d*=0.07824 which arbitrarily makes the visibility approach *VR*=50km as *CMass* and [NO_2] go to zero.

Fig.8.1 plots the visibility at the Liverpool, NSW site calculated with Yi et al [25] Model I and the coefficient *d*=0.07824. The dots are the daily data for the study period from 2017 to 2020 with the relative humidity *RH* averaged over each sampling 24 hour sampling day. The black triangles have every day fixed at *RH*=60% and the orange circles fixed at *RH*=80% for every sampling day. This graph shows clearly the strong influence that *RH* has on the visible range for PM2.5 *CMass*< 50µg/m^3. For lightly loaded days with say PM2.5 *CMass*=10 µg/m^3 the visibility ranges from 25 km to over 50km when *RH* ranges from 60% to 80%.

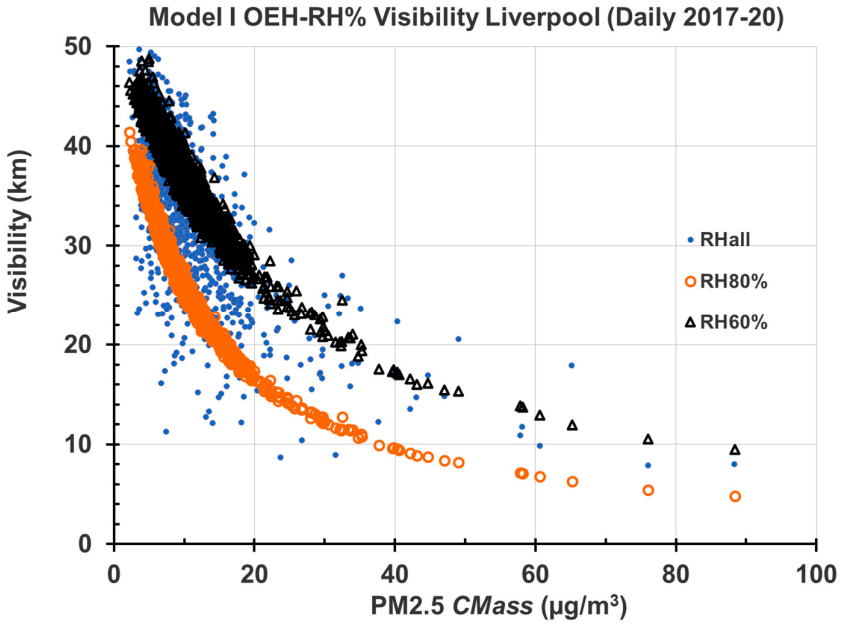

Fig. 8.1. Plot of visible range against PM2.5 CMass at Liverpool using Yi et al 2020 [25] with NSW OEH data with fixed relative humidity RH=80% and 60%for everyday and RHall has the RH for each individual day during the study period 2017-20.

We also see that for low mass concentrations below *CMass*<20 µg/m^3 the PM2.5 mass concentration is not an accurate predictor of visible range. The visibility range changes

too quickly in this region. For *CMass*> 20 µg/m^3 PM2.5 concentrations are a more accurate predictor of visual range If the relative humidity is well determined.

9. Summary

In this document we have discussed and defined the key parameters and terms that are directly related to determining the light extinction coefficient b_{ext}, light absorbing carbon (*LAC*), black carbon(*BC*) and visible range (*VR*). We have;

- provided the relationships and equations needed to determine and quantitatively measure and estimate these parameters,
- discussed most of the key assumptions and corrections that researchers have applied to these parameters
- provided graphs and tables containing typical values for these parameters as well as the numbers needed in the accurate determination of these parameters.

The focus here has been on transmission measurements through filters used to collect fine particulate mass (PM2.5) containing carbon. We appreciate that there are at least two significant forms of carbon on such filters, elemental carbon (*EC*) and organic carbon (*OC*). We have not addressed aspects associated with the measurement of organic carbon.

There are hundreds of journal papers discussing *LAC* published covering over 50 years of research The references provided below are absolutely the key references that should be read in detail. They provide a comprehensive overview of the understanding and measurement of b_{ext}, *LAC*, *BC* and *VR* and summarise the current thinking on these topics.

10. Acknowledgements

We are pleased to acknowledge the expertise of David Button in the manufacture and construction of the MABI unit and Dr A. Atanacio, Dr M. Manohar, P. Chatfield and C. Thompson in the operation of the MABI unit used for many of the black carbon data used in this report.

11. References

[1]. B.A.J. Ammerlaan, R. Holzinger, A.D. Jedynsk, J.S. Henzing, Technical note: Aerosol light absorption measurements with a carbon analyser Calibration and precision estimates. Atmospheric Environment, 164 (2017) 1-7.

[2]. W. Patrick Arnott , Khadeejeh Hamasha , Hans Moosmüller , Patrick J. Sheridan & John A. Ogren. Towards Aerosol Light-Absorption Measurements with a 7-Wavelength Nethalometer: Evaluation with a Photoacoustic Instrument and 3-Wavelength Nephelometer. https://doi.org/10.1080/027868290901972 Aerosol Science and Technology, 39 (2005) 17–29.

[3]. Tami C. Bond and Robert W. Bergstrom. Light Absorption by Carbonaceous Particles: An Investigative Review. https://doi.org/10.1080/02786820500421521 Aerosol Science and Technology, 40 (2006) 27–67.

[4]. G. P. Box, T Hallal, Optical properties of Sydney aerosols. Journal of Southern Hemisphere Earth Systems Science, 69 (2019)65-74.

[5]. P. M. Davey, A. H. Tremper, E. M. G. Nicolosi, P. Quincey, G. W. Fuller. Estimating particulate BC concentrations using two offline light absorption methods applied to four types of filter media. Atmospheric Environment, 152 (2017)24-33.

[6]. W. D. Dick, P. J. Ziemann and P. H. McMurry. Multiangle light scattering measurements of refractive index of submicron atmospheric particles. Aerosol Science and Technology 41 (2007) 549-569.

[7]. M Greilinger, L. Drinovec, G. Mocnik. A. Kasper-Giebl. Evaluation of measurements of light transmission for the determination of BC on filters from different station types. Atmospheric Environment, 198 (2019)1-11.

[8]. H.Horvath, Atmospheric light absorption – A Review. Atmospheric Environment 27 (1993) 293-317.

[9]. H. Horvath, Experimental calibration for aerosol light absorption measurements using the integrating plate method – Summary of the data, Aerosol Science, 28 (1997)1149-1161.

[10]. H. Horvath. Comparison of the light absorption coefficient and carbon measures for remote aerosols: An independent analysis of the data from the IMPROVE Network I and II., Atmos. Environ., 31 (1997b) 2885-2887.

[11]. Denghui JI, Zhaoze Deng, Xiaoyu Sun, Liang Ran, Xiangao Xia, Disong Fu, Zijue Song Pucai Wang, Yunfei Wu, Ping Tian, and Mengyu Huang. Estimation of PM2.5 Mass Concentration from Visibility. Advances in Atmospheric Sciences, 37 (2020) 671–678.

[12]. W. C. Malm, J.F. Sisler, D. Huffman, R.A. Eldred, T.A. Cahill, Spatial and seasonal trends in particle concentrations and optical estimations in the US, J.Geophys. Res., 99 (1994) 1347-1370.

[13]. W. Maenhaut, Ghent University, Ghent, Belgium, private communication, 1998.

[14]. Nicola Masey, Eliani Ezani, Jonathan Gillespie, Fiona Sutherland, Chun Lin, Scott Hamilton, Mathew R. Heal, Iain J. Beverland. Consistency of Urban Background Black Carbon Concentration Measurements by Portable AE51 and Reference AE22 Aethalometers: Effect of Corrections for Filter Loading. Aerosol and Air Quality Research, 20 (2020) 329–340.

[15]. H. Moosmuller, R.K.Chakrabarty, W.P.Arnott. Aerosol light absorption and its measurement: A review. Journal of Quantitative Spectroscopy and Radiative Transfer 110 (2009) 844–878.

[16]. A. Mousavi, M. H. Sowlat, C. Lovett, M. Rauber, S. Szidat, R. Boeffi, A. Borgini, C de Marco, A. A. Ruprecht, C. Sioutas. Source apportionment of BC from fossil fuel and biomass burning in metropolitan Milan, Italy. Atmospheric Environment 203 (2019) 252-261.

[17]. M. Pitchford,W. C. Malm, B. Schichtel, N. Kumar, D. Lowenthal, J. Hand. Revised Algorithm for Estimating Light Extinction from IMPROVE Particle Speciation Data. J. Air and Waste Manage. Assoc. 57 (2007) 1326–1336.

[18]. A.W.Strawa, T.W.Kirchstetter, A.G.Hallar, G.A.Ban-Weiss, J.P.McLaughlin, R.A. Harley, M.M.Lunden. Optical and physical properties of primary on-road vehicle particle emissions and their implications for climate change. Journal of Aerosol Science 41 (2010) 36–50

[19]. Xiaoyun Sun, Tianliang Zhao, Duanyang Liu, Sunling Gong, Jiaping Xu and Xiaodan Ma. Quantifying the Influences of PM2.5 and Relative Humidity on Change of Atmospheric Visibility over Recent Winters in an Urban Area of East China. Atmosphere 11 (2020) 461-483.

[20]. G. Taha, G. P. Box, D. D. Cohen, E. Stelcer. Black Carbon Measurement using Laser Integrated Plate Method. Aerosol Science and Technology, 41 (2007) 266-276.

[21]. Thomas W. Kirchstetter, T. Novakov. Controlled generation of black carbon particles from a diffusion flame and applications in evaluating black carbon measurement methods. Atmospheric Environment 41 (2007) 1874–1888.

[22]. Jun Tao, Leiming Zhang, Kinfai Ho, Renjian Zhang, Zejian Lin, Zhisheng Zhang, Mang Lin, Junji Cao, Suixing Liu, Gehui Wang. Impact of PM2.5 chemical compositions on aerosol light scattering in Guangzhou — the largest megacity in South China. Atmospheric Research 135–136 (2014) 48–58.

[23]. Warren H. White, Krystyna Trzepla, Nicole P. Hyslop and Bret A. Schichtel, A critical review of filter transmittance measurements for aerosol light absorption, and de novo calibration for a decade of monitoring on PTFE membranes. Aerosol Science and Technology, 50:9 (2016) 984-1002, DOI: 10.1080/02786826.2016.1211615

[24]. E. Weingartnera, H. Saatho, M. Schnaiter, N. Streit, B. Bitnar, U. Baltensperger. Absorption of light by soot particles: determination of the absorption coeffcient by means of aethalometers. Aerosol Science 34 (2003) 1445–1463.

[25]. Hui Yi, Jingjing Zhang, Hang Xiao, Lei Tong, Qiuliang Cai, Jiamei Lin, Weijia Yu, Matthew S. Johnson. Compact Algorithms for Predicting the Atmospheric Visibility Using PM2.5, Relative Humidity and NO_2. Aerosol and Air Quality Research, 20 (2020) 679–687.

[26]. Yunfei Wu, Peng Yan, Ping Tian, Jun Tao, Ling Li, Jianmin Chen, Yangmei Zhang, Nianwen Cao, Chong Chen, Renjian Zhang. Spectral Light Absorption of Ambient Aerosols in Urban Beijing during Summer: An Intercomparison of Measurements from a Range of Instruments. Aerosol and Air Quality Research, 15 (2015) 1178–1187.

[27]. Hujia Zhao, Huizheng Che, Xiaoye Zhang, Yanjun Ma, Yangfeng Wang, Hong Wang, Yaqiang Wang. Characteristics of visibility and particulate matter (PM) in an urban area of Northeast China. Atmospheric Pollution Research 4 (2013) 427-434.

12. Appendix 1 Glossary

#	Symbol	Term	Comments
	A	Filter collection area (cm^2)	
	ANSTO	Australian Nuclear Science and Technology Organisation	
	ASP	Aerosol Sampling Network pram in ANSTO	
	ATN	*Ln* of the absorption term	Equ. 2.8
	α	Angstrom exponent	Equ. 4.1
	α_{ff}	Angstrom exponent for fossil fuel combustion	
	α_{bb}	Angstrom exponent for biomass burning	
	b_{abs}	light absorption coefficient (Mm^{-1})	Equ. 2.7
	b_{abs}^{corr}	b_{abs} corrected for scattering and particle loading	Equ. 2.9
	b_{ext}	light extinction coefficient (Mm^{-1})	Equ. 2.6
	b_{scat}	light scattering coefficient (Mm^{-1})	
	BC	Light absorbing carbon corrected for soil – called black carbon.	Equ. 3.7
	C	Scattering correction to b_{abs}	Equ. 2.10
	CMass	Mass per unit volume (µg/m3)	
	D	Particle diameter	
	EC	Elemental carbon	
	ϵ	Uncorrected mass attenuation coefficient (m^2/g)	Equ. 3.1
	ε, ε^{corr}	Corrected mass attenuation coefficient (m^2/g)	Equ. 3.3
	EC	Elemental carbon	
	HeNe	Helium/ Neon laser with wavelength 633nm	
	I	Transmission intensity after exposure	Equ. 2.5
	I_0	Transmission intensity before exposure	
	k	Compensation parameter	Equ. 2.15
	LAC	Light absorbing carbon (ng/m^3)	Equ. 3.2
	λ	Wavelength (nm)	
	m	Complex refractive index *m=n-ik*	
	MABI	Multiwavelength absorption black carbon instrument	
	MAC, MAE	Mass absorption coefficient, or efficiency (m^2/g)	
	N	Number of particles per unit volume ($particles/cm^3$)	Equ. 2.17
	N_o	Avogadro's number $6.022141x10^{23}$	
	NSW	New South Wales	
	OEH	Office of Environment and Heritage	
	OC	Organic carbon	
	pphm	Parts per hundred million	
	Q_i	Normalised efficiency factor for i=ext, scat or abs	Equ. 6.4
	R	Loading correction to b_{abs}	Equ. 2.11
	RH	Relative humidity (%)	
	ρ	Particle density (g/cm^3)	
	ρx	Particle thickness on filter ($\mu g/cm^2$)	Equ. 2.12

	σ_i	*i=ext, scat or abs* cross section (cm^2)	
	Soil	Soil estimate from oxides of Al, Si, Ti, Ca and Fe	Equ. 3.8
	τ	Aerosol optical depth	
	UCD	University of California Davis, California ,USA	
	V	Volume in which the particles were collected (m^3)	
	VR	Visible range (km)	Equ. 8.1
	ω_0	Single particle scattering albedo coefficient	Equ. 2.2
	W	Molecular weight (g)	
	x	Particle diameter normalised to wavelength	Equ. 6.2

Blank page